JCTC Journal of Chemical Theory and Computation

An Automated and Systematic Transition Structure Explorer in Large Flexible Molecular Systems Based on Combined Global Reaction Route Mapping and Microiteration Methods

Satoshi Maeda,[†,‡] Koichi Ohno,*[,‡] and Keiji Morokuma*[,†,§]

Department of Chemistry and Cherry L. Emerson Center for Scientific Computation, Emory University, Atlanta, Georgia 30322, Toyota Physical and Chemical Research Institute, Nagakute, Aichi 480-1192, Japan, and Fukui Institute for Fundamental Chemistry, Kyoto University, Kyoto 606-8103, Japan

Received July 4, 2009

Abstract: The global reaction route mapping (GRRM) method enabled an automated and a systematic search for routes of chemical reactions on a potential energy surface based on the anharmonic downward distortion following (ADDF) approach [*Chem. Phys. Lett.* **2004**, *384*, 277]. On the other hand, the microiteration technique [*Mol. Phys.* **2006,** *104*, 701] has been developed for full optimizations of transition state (TS) structures for reactions/transformations in large flexible molecular systems and successfully used in ONIOM(QM:MM) calculations. In the present paper, combining the GRRM method with the microiteration technique, we developed a microiteration-ADDF (μ-ADDF) method for automated and systematic TS exploration of large flexible molecular systems. We showed that the method works well with two test systems, $(H_2CO)(H_2O)_{100}$ and $Si_6(C_{12}H_{17})_6$, in the ONIOM(QM:MM) framework. It is noted that the present μ-ADDF method can be used for pure quantum mechanics (QM) or molecular mechanics (MM) systems (without ONIOM) and has been tested successfully in $C_6H_{10}O$ pure QM calculations.

I. Introduction

Determination of transition state (TS) structures, first-order saddle points on a potential energy surface (PES), is essential in theoretical studies of chemical reaction mechanisms.[1,2] Quantum mechanics/molecular mechanics (QM/MM)[3−5] and the more general ONIOM[6−8] approaches made applications of accurate quantum methods, such as ab initio and density functional methods, possible to very large molecular systems including biological molecules. For discussing reaction mechanisms in such systems, a search is required for TS structures of chemical bond rearrangements in a given reaction center region surrounded by large substituents or environmental systems such as protein.

* Corresponding authors. E-mail: ohnok@mail.tains.tohoku.ac.jp (K.O.) and morokuma@emory.edu (K.M.).

† Emory University.

‡ Toyota Physical and Chemical Research Institute.

§ Kyoto University.

The Newton−Raphson method or the more sophisticated augmented Hessian approaches, such as the Berny optimization algorithm[9] and the eigenvector following[10] (EF) and the rational function optimization[11] (RFO) methods, are employed in TS optimizers. Efficiency of these methods strongly depends on the overall algorithm including the selection of coordinate system,[12−14] the Hessian update scheme,[15−18] the use of the trust radius for limiting step size,[19−21] and so on.[1] Obviously, standard Hessian-based approaches are not applicable to very large molecular systems without special care because of the following two difficulties: (1) quadratic and cubic increase of Hessian storage and diagonalization costs, respectively, with respect to the numbers of atoms N, and (2) selecting initial geometries with only one imaginary frequency eigenvector parallel to desired reaction routes from extensive coordinate space of such systems.

Both of the above two difficulties can be greatly circumvented by use of the microiteration technique.[22−28] In a geometry optimization algorithm based on the microiteration

10.1021/ct9003383 CCC: $40.75
Published on Web 09/04/2009

technique in ONIOM or QM/MM method, optimizations of MM atom positions fixing all QM atoms (microiteration) are performed before every optimization step of QM atom positions (macroiteration). Since MM atom positions can be removed from optimization variables in macroiterations, this algorithm greatly simplifies the problem preparing initial structures with the correct Hessian structure. The difficulty concerning the size of a Hessian matrix is completely removed in microiterations because first-order optimization techniques, such as the conjugated gradient method, can be employed in microiterations. Although many more force calculations will be required in first-order methods than in second-order methods, which use (exact or updated) Hessian, this does not matter in microiterations since the cost of force calculations is trivial in MM calculations. In the microiteration method, the coupling of both the QM and MM parts is usually completely neglected in the QM Hessian calculation. Recently, a fully coupled optimization algorithm was proposed in which quadratic couplings between the QM and MM regions are taken into account explicitly in macroiterations,[29] and it dramatically reduced the number of macroiteration steps. Although the first difficulty again arises in the fully coupled scheme since diagonalization of full Hessian matrices, including QM/QM, QM/MM, and MM/MM terms, is required in every macroiteration to take the quadratic couplings into account, its cost can be reduced to O(N) scaling by using sophisticated numerical techniques, such as the iterative Davidson diagonalization[30] algorithm and the fast multipole[31,32] method.[29] This fully coupled microiteration scheme implemented in a development version of Gaussian and recently released Gaussian 09[33] programs enabled efficient full optimization of ONIOM(QM:MM) TSs and intermediates of complex systems, such as the entire mechanism consisting of multiple steps for the nonheme iron enzyme isopenicillin N synthase containing as many as 5 368 atoms.[34]

Augmented Hessian methods, when used in general TS optimizers, maximize the energy in the direction of the only imaginary frequency eigenvector. Toward this goal, a user has to prepare a good initial guess, which already has a negative eigenvalue (or a lowest positive eigenvalue, which has eigenvector parallel to the negative eigenvalue direction at a final TS structure). Therefore, a method that does not require any initial guess of TS structures is desired to be combined with the microiteration technique to find all of the important TS structures for a chemical reaction. Here, two situations can be considered: (1) both reactant and product structures are known beforehand, and (2) only a reactant structure is available. In the first case, there are many good so-called double-ended methods,[35−43] and some of them can be applied to multistep cases without knowledge of all intermediates. One of them, the synchronous transit-guided quasi-Newton method[36] has already been used in combination with the microiteration technique in Gaussian programs, although it cannot be employed for multistep reactions unless one prepares a series of all intermediate structures beforehand. In the second case, one has to use one-point methods which gives all of the intermediates and the TSs automatically from only one input structure. There are three such approaches which have actually been applied to automated global mapping of ab initio PESs: (1) the gradient extremal following[44−53] (GEF), (2) the reduced gradient following[54−60] (RGF), and (3) the anharmonic downward distortion following[61−63] (ADDF). The former two have been applied to a system composed of only four atoms.[53,54] On the other hand, we proposed the global reaction route mapping (GRRM) method on the basis of the ADDF approach,[61−63] and the GRRM method enabled automated and systematic global mapping on PESs of given chemical formula in many small systems.[64−69] Hence, the GRRM should be the method of choice to be combined with the microiteration technique for exploring PESs of reaction center variables in large flexible environments.

II. Theory

The GRRM Method. If reaction routes can be followed in both uphill and downhill directions, then GRRM can be performed as follows: (1) an equilibrium (EQ) structure is optimized starting from an arbitrary input structure; (2) the optimized EQ is added to a list of EQ structures (EQ-list); (3) all entrances of reaction pathways are searched at one of EQs in the EQ-list; (4) each pathway is followed in an uphill direction toward a TS or a dissociation channel (DC); (5) starting from each TS obtained, an EQ is searched by following the reaction pathway in a downhill direction; (6) new EQs are added to the EQ-list; (7) return to (3) if there is any EQ in the EQ-list to which the procedures (3−6) have not yet been applied; and (8) exit from the cycle if not. A completion of this procedure is expected to give a global reaction route map including all EQs and TSs for a given chemical formula. Here, downhill walks from TSs can be performed by using conventional intrinsic reaction coordinate (IRC) following techniques.[70−73] Unfortunately, there is no technique which is mathematically guaranteed to find out all entrances of reaction pathways from an EQ structure. Recently, we suggested a principle that all reaction pathways can be found as ADD maxima around EQ points.[61−63] Although this is not a mathematical theorem either, we have shown that it worked very well in many previous applications.[64−69] Hence, we proposed the GRRM method using both uphill (ADDF)[61−63] and downhill (IRC)[70−73] methods.

Some approximate treatments of the GRRM method can be considered in which the procedures (3−6) are applied to only selected EQs, which are important in a specific problem. For instance, they are applied to only stable EQs or TSs with less than a given total energy, or they are applied to only EQs possessing a specified bonding pattern. All of these treatments are available in the latest version of the GRRM program.

The ADDF Approach. Many typical potential curves show a common feature that potential energy always becomes lower than the harmonic potential defined at the bottom of the curves in directions leading to DCs and TSs. From this feature, we proposed a principle that reaction channels can be found by following ADD maxima starting from an EQ structure on a PES.[61−63] In other words, existence of a flat region of PES or another EQ should have a certain influence upon PES around the starting EQ, and such indications can

be detected as ADD maxima at the starting EQ. In many previous applications, the GRRM method based on the ADDF approach has found many unknown as well as (almost) all known reaction channels automatically.[61−69] The ADD maxima can be detected in multidimension by using the scaled hypersphere search (SHS) technique as explained below.

There are many local ADD maxima around a starting EQ, and in the full-ADDF (*f*ADDF) approach all of them are followed.[61−69] We suggested that larger ADDs are related to lower barrier pathways leading to lower energy EQs,[74] by combining the Bell−Evans−Polanyi (BEP) principle[75,76] with the above ADD principle. The BEP principle tells that the deeper minimum of the product side is related to the lower barrier, whereas the ADD principle says that the deeper minimum (strong potential lowering interaction) of the product side is related to the larger ADD of the reactant side. It follows that the larger ADD is related to the lower barrier leading to the deeper minimum, and high barrier pathways can be omitted by comparisons of magnitude of ADDs at the starting EQ without following them. In the large-ADDF[74] (*l*ADDF) approach, one follows only large ADDF pathways avoiding those suggesting high barriers; this approach has been applied to H-bond cluster systems[74,77−79] and conformation samplings.[80,81]

The SHS Technique. ADD maxima are searched by comparisons between harmonic and real (QM, MM, or QM/MM) energies on an isoenergy hypersurface of harmonic potential. Such a hypersurface is a hyperellipsoid centered at the starting EQ and can be converted to a simple hypersphere if the scaled normal coordinates $q_i = \lambda_i^{1/2} Q_i$ are employed, where λ_i is the eigenvalue of Q_i. In the SHS technique, ADD maxima can be detected as energy minima on the scaled hyperspheres, and they are traced by expanding the hypersphere radius. The method to find all or *n*-lowest ADDs on a given scaled hypersphere was discussed in the previous papers[62,74] and will not be repeated. Here, use of the harmonic reference is essential in the ADDF by the SHS method, and how to define a good harmonic reference for reaction center variables was a key point of the present development.

An angle coordinate (θ_1, θ_2, ..., θ_{f-1}) is used as variables in the energy minimizations on the scaled hyperspheres with a given radius r (in hartree$^{1/2}$) as in the polar coordinate interpolation.[82] In the latest implementation, (θ_1, θ_2, ..., θ_{f-1}) are defined using a set of orthogonal vectors ($\mathbf{u}_1$, $\mathbf{u}_2$, ..., $\mathbf{u}_{f-1}$, $\mathbf{v}$) as $f = 3N - 6$ axes. At first, a Cartesian Hessian (exact or updated) is converted to the one in the scaled normal coordinate. This is a simple coordinate rotation and scaling. Here, $\mathbf{v}$ is a unit vector pointing to the present position from the origin (starting EQ), and projections of $\mathbf{v}$ are eliminated from the Hessian by using the projection method.[83] Then, diagonalization of the projected Hessian gives $f - 1$ eigenvectors $\mathbf{u}_i$ with nonzero eigenvalues ε_i. Based on an expansion at the present position with $\theta_i = 0$ for all i, u_i, and v at other points on the sphere can be written as

$$\begin{aligned} u_i &= r\sin\theta_i \prod_j^{i-1} \cos\theta_j \\ v &= r \prod_j^{f-1} \cos\theta_j \end{aligned} \tag{1}$$

From eq 1, $\partial u_i/\partial\theta_i = r$, $\partial u_i/\partial\theta_j = 0$ ($i \neq j$), $\partial^2 u_i/\partial\theta_j\partial\theta_k = 0$, $\partial v/\partial\theta_i = 0$, $\partial^2 v/\partial\theta_i^2 = r$, $\partial^2 v/\partial\theta_i\partial\theta_j = 0$ ($i \neq j$) can be obtained at the present position with $\theta_i = 0$ for all i. Then, these conditions and $\partial^2 E/\partial u_i \partial u_j = 0$ ($i \neq j$) give

$$\begin{aligned} \frac{\partial E}{\partial \theta_i} &= r\frac{\partial E}{\partial u_i} \\ \frac{\partial^2 E}{\partial \theta_i^2} &= r^2\varepsilon_i + r\frac{\partial E}{\partial v} \end{aligned} \tag{2}$$

Here, Hessian in terms of θ_i is already diagonal, i.e., $\partial^2 E/\partial\theta_i\partial\theta_j = 0$ ($i \neq j$), without further diagonalization, and $\partial E/\partial\theta_i$ and $\partial^2 E/\partial\theta_i^2$ are used as gradient components and Hessian eigenvalues in an optimizer in the GRRM program based on the RFO and trust radius methods.

Double-Ended Methods in the GRRM Program. We also have a double-ended method in the GRRM program, which requires two initial structures but is much faster than the one-point method in general, since the area to be searched can be limited to a small region between the two structures.[42,43] In the double-ended ADDF (*d*ADDF) method, energy minima on the scaled hyperspheres are followed in the reverse direction from a point on a very large hypersphere to the sphere center with reducing hypersphere radius. If there exists only one TS between the two structures, the trace of ADD maximum points is expected to pass through the TS region, same as the original sphere expansion ADDF algorithm. Hence, the *d*ADDF can be used as a guide to a TS region between two adjacent EQs, which we call *d*ADDF-guided TS search (*d*ADDF-TS) approach.[42] On the other hand, if there exists many EQ structures between the two chosen starting structures, a harmonic reference defined at a sphere center is no longer meaningful at a very long distance from the sphere center. In such a case, the trace of ADD maximum points may not pass through TS regions. However, each EQ (minima in *f* dimension) are still on the traces of minima on hyperspheres (minima in $f - 1$ dimension) followed by the *d*ADDF, and the *d*ADDF will give many EQs (intermediates) along its traces, where we call this procedure as *d*ADDF-guided EQ search (*d*ADDF-EQ) approach.[43] It is not guaranteed that all intermediates are obtained by only one application of the *d*ADDF-EQ to highly multistep and/or highly curved pathways, and one has to add some EQs by further applications of the *d*ADDF-EQ to pairs of EQs obtained in the initial application.[43] Finally, one can find a set of TSs connecting the intermediates by applying *d*ADDF-TS method to adjacent pairs in a set of EQs prepared by the *d*ADDF-EQ.

Effective Gradient and Hessian in the *μ*-ADDF Algorithm. We assume that there are p ($= 3N - 6$) reaction-center variables x (coordinates directly involved in the reaction) and q ($= 3M$) nonreaction-center variables y in a system composed of $N + M$ atoms. A second-order potential function for this system can be written as

$$V = \varepsilon_0 + \sum_i^p g_i^R x_i + \frac{1}{2}\sum_i^p \sum_j^p h_{ij}^R x_i x_j + \frac{1}{2}\sum_i^p \sum_j^q h_{ij}^C x_i y_j + \frac{1}{2}\sum_i^q \sum_j^p h_{ij}^C y_i x_j + \frac{1}{2}\sum_i^q \sum_j^q h_{ij}^N y_i y_j \quad (3)$$

where g^R are gradients for reaction-center variables, h^R, h^N, and h^C are Hessian matrix elements for reaction-center and nonreaction-center variables and their couplings, respectively. Here, all gradient components for nonreaction-center variables g^N are zero because they are already optimized in microiteration. In macroiterations, PESs of reaction-center variables fulfilling the following condition for nonreaction-center variables is considered

$$\frac{\partial V}{\partial y_n} = \sum_j^p h_{nj}^C x_j + \sum_j^q h_{nj}^N y_j = 0 \quad (4)$$

We rewrite eq 4 as the following simultaneous equations:

$$\sum_j^q h_{nj}^N y_j = -\sum_j^p h_{nj}^C x_j \quad (5)$$

Solutions of eq 5 for nonreaction-center variables are

$$y_m = -\sum_n^q \sum_j^p \gamma_{nm}^N h_{nj}^C x_j \quad (6)$$

where γ^N are elements of inverse Hessian matrix for nonreaction-center variables. On the other hand, the following condition can be obtained when summation over n is taken for eq 5 multiplied by y_n.

$$\sum_n^q \sum_j^q y_n h_{nj}^N y_j = -\sum_n^q \sum_j^p y_n h_{nj}^C x_j \quad (7)$$

From eq 7, the fifth and sixth terms in eq 3 are canceled out. Then, substitution of eq 6 into eq 3 without the fifth and sixth terms gives an effective second-order potential for reaction-center variables as

$$V = \varepsilon_0 + \sum_i^p g_i^R x_i + \frac{1}{2}\sum_i^p \sum_j^p h_{ij}^R x_i x_j - \frac{1}{2}\sum_i^p \sum_m^q \sum_n^q \sum_j^p h_{im}^C \gamma_{nm}^N h_{nj}^C x_i x_j \quad (8)$$

This tells that the effective gradients for reaction-center variables are identical to the original gradients without any correction, and effective Hessian matrix elements for reaction-center variables can be obtained as

$$\frac{\partial^2 V}{\partial x_i \partial x_j} = h_{ij}^R - \sum_m^q \sum_n^q h_{im}^C \gamma_{nm}^N h_{nj}^C \quad (9)$$

Implementation of the Microiteration Technique in the GRRM Program. We implemented an interface with ONIOM in a previous version of GRRM program.[80] However, the *l*ADDF algorithm there worked only in conformation samplings of flexible parts in large systems because the ADDs related to conformation changes (with only a few kJ/mol barriers) are much larger than the ones for chemical bond reorganization (typically with more than 10 kJ/mol barriers). Although, in principle, the *f*ADDF can find out all reaction routes, including chemical bond rearrangement pathways, it is not applicable in practice to very large systems. By combining with the microiteration technique, the *f*ADDF and *l*ADDF can be a practical automated TS explorer for chemical bond rearrangement reactions in large flexible systems. In the present implementation, all movements of reaction-center atoms were treated by the GRRM program as in the case without microiterations, where g^R and the (exact or updated) effective Hessian were employed for determining each displacement of atoms. Before every macroiterations (in minimizations on scaled hyperspheres, EQ and TS optimizations and IRC followings), positions of nonreaction-center atoms were optimized by using a microiteration code in the Gaussian programs, where opt = tight criterion was employed. All μ-ADDF algorithms, i.e., μ-*f*ADDF, μ-*l*ADDF, and μ-*d*ADDF, are now available in our GRRM program coupled with the Gaussian programs (only 03[84] and 09[33] versions).

It is noted that the microiteration technique is not necessarily limited to the ONIOM method. Division of the reaction-center and nonreaction-center variables can be made also within a pure QM system, a pure MM system, or a different division scheme from the ONIOM model real division.

As shown in eq 8, g^R is already including quadratic couplings with nonreaction-center variables implicitly. Hence, quadratic couplings are fully taken into account also in updated Hessian for reaction-center variables. It is known that usual Hessian update schemes by using g^R can be unstable when different coordinates are used for different parts,[29] e.g., redundant internal coordinates,[12−14] and Cartesian coordinates are used for reaction-center and nonreaction-center variables, respectively, in Gaussian programs. In the SHS technique, as discussed above, we use the angle coordinate for energy minimization on the scaled hyperspheres, and the same problem would happen if Hessian was updated in the angle coordinate. However, as explained above, we start with Cartesian Hessian (updated in Cartesian coordinate) in the process for determining minimization steps. Since microiterations are also performed in Cartesian coordinate in the Gaussian programs, we have never suffered from the instability problem in Hessian updates.

Only when exact Hessian is computed, a transformation of full-Hessian (including all of h^R, h^N, and h^C terms) into the effective Hessian of eq 9 is needed, where, in the present applications, exact Hessian was computed at the starting EQ point in the ADDF, every 50 macroiterations in both minimizations on scaled hyperspheres and macroiterations in EQ optimizations, every 5 macroiterations in TS optimizations, and every 10 macrosteps of IRC followings. In this transformation, we need the inverse matrix of Hessian for nonreaction-center variables. Here, we rewrite eq 9 as

$$\frac{\partial^2 V}{\partial x_i \partial x_j} = h_{ij}^R - \mathbf{h}_i^t \mathbf{H}_N^{-1} \mathbf{h}_j \quad (10)$$

where $\mathbf{h}_i = (h_{i1}^C, h_{i2}^C, ..., h_{iq}^C)$, and $\mathbf{H}_N$ is Hessian matrix for nonreaction-center variables. We have to perform either inversion of $\mathbf{H}_N$ or p time evaluations of $\mathbf{w}_j = \mathbf{H}_N^{-1}\mathbf{h}_j$. A

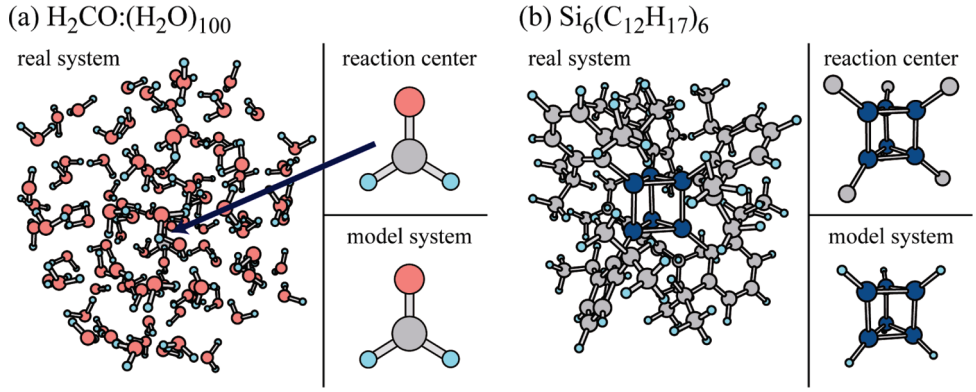

Figure 1. Definitions of real system, reaction-center, and ONIOM model system in the present applications to (a) $(H_2CO)(H_2O)_{100}$ and (b) $Si_6(C_{12}H_{17})_6$.

matrix inversion requires $O(q^3)$ costs, in general, whereas one $\mathbf{w}_j$ can be obtained by the iterative conjugate gradient method with (potentially) much less CPU time. Since p is much smaller than q, in general, and storage of p $\mathbf{w}_j$ vectors is trivial, the latter is used in this study. The most time-consuming part in the conjugate gradient method is the calculation of a product of $\mathbf{H}_N$ with an approximate vector for $\mathbf{w}_j$ in each iteration. Its cost can be reduced to $O(q)$ from $O(q^2)$ by a direct algorithm proposed recently.[29] This transformation requires $O(q^2)$ memory to keep $q \times q$ matrix elements of $\mathbf{H}_N$: ~0.45 GB for $M = 2\,500$ atoms ($q = 7\,500$), ~1.8 GB for $M = 5\,000$ atoms ($M = 15\,000$), ~7.2 GB for $M = 10\,000$ atoms ($q = 30\,000$). Hence, this transformation is trivial (relative to QM/MM Hessian calculations) in recent computers when nonreaction-center atoms are less than 5 000, although QM/MM Hessian calculation itself will be expensive in such large molecules. Memory size for this transformation also can be reduced significantly if the direct algorithm[29] is employed in the future. An $O(N)$ approach with iterative algorithm and inverse Hessian update for eigenvalues and eigenvectors search introduced in an earlier paper[85] will solve this problem as well.

III. Numerical Tests

In this paper, we show three numerical examples. The first two, for systems shown in Figure 1, are ONIOM applications in which the ONIOM model system is assumed to be the same as the μ-ADDF reaction center. One is reactions of formaldehyde surrounded by 100 water molecules with H_2CO as the ONIOM QM model system and the microiteration reaction center. Another is reactions of hexasilaprismane[86−88] in which Si_6C_6 are treated as reaction-center atoms in the microiteration, whereas Si_6H_6 with link H atoms is a ONIOM QM model system. The third example is a pure QM calculation for cyclohexanone (a cyclic ketone molecule with a C_6 ring) at the semiempirical PM3 level, where a carbonyl group and two carbons connected to the carbonyl group ($C_2C{=}O$) were treated as reaction-center atoms. Performance of the μ-ADDF calculations for the real systems was compared with performance of the ADDF calculations for the model systems.

$(H_2CO)(H_2O)_{100}$ in ONIOM. Total energy, gradient, and Hessian were computed by the ONIOM(HF/6-31G:AMBER) method by using the Gaussian program. Here, MM charges on H_2CO and H_2O are the natural charges of the isolated molecule and the original TIP3P parameters,[89] respectively, and they are mechanically embedded in the ONIOM calculations. The initial EQ structure was prepared as follows: (1) the center-of-mass position of H_2CO at HF/6-31G level was set to the origin, (2) one hundred water molecules with both random center-of-mass positions and orientations were distributed in a sphere centered at the origin, and (3) geometry optimization was performed from the structure of (2) by using an optimizer in the GRRM program coupled with the Gaussian microiteration code. Then, the μ-*f*ADDF method was applied to this initial EQ structure. To see validity of the effective Hessian in eq 10, an μ-*f*ADDF calculation with uncorrected Hessian (h^R in eq 10) was also performed for comparison. If the present μ-*f*ADDF algorithm worked very well, then the numbers of macroiterations will be comparable to the numbers of total cycles in the *f*ADD calculation for H_2CO, and the latter calculation at HF/6-31G level was also performed for comparison.

Table 1. Harmonic Frequencies (in cm^{-1}) of the Effective Reaction-Center Hessian (H^{eff}) of $(H_2CO)(H_2O)_{100}$ for the Uncorrected Reaction-Center Hessian (h^R) of $(H_2CO)(H_2O)_{100}$ and for H_2CO

	effective Hessian, eq 10	uncorrected Hessian, h^R in eq 10	Hessian for H_2CO only
ω_1	1 332	1 348	1 329
ω_2	1 371	1 392	1 374
ω_3	1 675	1 690	1 674
ω_4	1 903	1 906	1 910
ω_5	3 170	3 226	3 208
ω_6	3 300	3 318	3 299

Table 1 compares harmonic frequencies of the effective Hessian, the uncorrected Hessian, and the model system. As seen in this table, frequencies of the effective Hessian are very similar to the ones for the model system, and differences in ω_1, ω_2, ω_3, and ω_6 are only 1−3 cm^{-1}. Although ω_4 (CO stretch) and ω_5 (symmetric CH stretch) show relatively large deviations, this may be because these two modes, especially ω_5, change the volume of H_2CO significantly, and such movements were suppressed by the surrounding waters. On the other hand, the uncorrected Hessian overestimates all the frequencies compared to those of the effective Hessian. This is because an energy-lowering effect via the microiteration

Table 2. Performance of the μ-*f*ADDF for $(H_2CO)(H_2O)_{100}$ Compared to the μ-*f*ADDF with the Uncorrected Hessian and the *f*ADDF for the Model System

	μ-*f*ADDF with effective Hessian, eq 10	μ-*f*ADDF with uncorrected Hessian, h^R in eq 10	*f*ADDF for H_2CO only
n_{ADD}	9	14	9
$n_{gradient}$	2 665	5 741	2 482
$n_{Hessian}$	117	192	101

(energy minimization for the nonreaction-center atoms) is omitted in the uncorrected Hessian, whereas it is correctly included in the effective Hessian via the quadratic couplings. How these frequency differences of $3-56\ cm^{-1}$ (0.16−1.8%) affect the performance of the μ-*f*ADDF will be discussed below.

Table 2 compares performance of the μ-*f*ADDF with the effective Hessian, the μ-*f*ADDF with the uncorrected Hessian, and the *f*ADDF for the model system. Here, in all cases, a TS for both dissociation into H_2 + CO and isomerization into hydroxymethylene were obtained. As expected, μ-*f*ADDF with the effective Hessian showed almost the same performance as the model system. Exactly the same numbers of ADDs with the same characters were followed in these two cases: two isomerization pathways to hydroxymethylene via a TS, two direct dissociation routes to H + HCO, one direct dissociation route to O + CH_2, two dissociation routes to H_2 + CO via a TS, and two dissociation routes to H_2 + CO via a non-TS region with symmetric out-of-plane motion. The numbers of both QM gradient and Hessian calculations are also very similar to each other in these two cases. Although the μ-*f*ADDF required bit more QM gradient and Hessian, this is because $(H_2CO)(H_2O)_{100}$ is not invariant against permutation of two H atoms in H_2CO. This symmetry breaking gives two independent TSs for migration of each H atom in the isomerization to hydroxymethylene and also two independent TSs for asymmetric association of two H atoms in the dissociation to H_2 + CO. Only two IRC calculations were required in the model system, whereas four calculations were required in the μ-*f*ADDF case, since the IRC calculation is performed when an independent TS is found. This can be seen from the $n_{gradient}$ as well as $n_{Hessian}$ ratios between these two cases which are 1.07 and 1.16, respectively. As explained above, we perform Hessian calculations with a higher frequency in IRC calculations, and hence, the higher ratio in $n_{Hessian}$ implies that the difference was not caused in the ADDF process. It follows that the present μ-*f*ADDF code coupled with a microiteration code in the Gaussian programs worked nearly perfectly in this very simple numerical test.

Only 0.16−1.8% overestimation of the harmonic frequencies in the μ-*f*ADDF with the uncorrected Hessian caused substantial deterioration in performance of the ADDF. Five extra pathways were followed via non-TS regions, and this increased the total numbers of gradient calculations to more than double. This is because minima on the scaled hyperspheres, based on wrong harmonic frequencies, are no longer ADD maximum points. This demonstrates how important the good harmonic reference is in the ADDF approach.

Another point we have to discuss here is that IRC calculations in the reverse direction from obtained TSs sometimes (three out of four TSs) did not come back to the initial EQ but lead to EQs for $(H_2CO)(H_2O)_{100}$ with other $(H_2O)_{100}$ arrangements. $(H_2CO)(H_2O)_{100}$ has numerous local structures with different $(H_2O)_{100}$ arrangements, and some of them are connected to one of the four TSs, while others are not. If one had to prepare correct $(H_2O)_{100}$ arrangements for each bond rearrangement, then the problem was much more complicated. However, fortunately, our observation in this test is that the μ-ADDF was able to find out all of the four TSs starting from an arbitrary $(H_2O)_{100}$ arrangement, which does not have direct connection to all four in full-dimension. This may be because small changes in the $(H_2O)_{100}$ arrangement caused only negligible effects on the reference harmonic frequencies of the reaction-center variables. No significant bumps were detected along traces of ADDs due to changes in $(H_2O)_{100}$ arrangements. A similar thing was also observed in the $Si_6(C_{12}H_{17})_6$ case. Hence, to our recommendation, one does not need to prepare a conformation of the nonreaction center parts with a direct connection to a final TS, but it is better to start from a conformation preferred at a given experimental condition or an experimental structure.

$Si_6(C_{12}H_{17})_6$ in ONIOM. Total energy, gradient, and Hessian were computed by the ONIOM(B3LYP/6-31G(d):UFF) method by using the Gaussian program. The initial EQ structure and MM-charges were prepared as follows: (1) a conformation sampling for the hydrocarbon arrangements with freezing the Si_6-cage structure was performed by using the *l*ADDF method and the UFF force-field with zero MM-charges on the hydrocarbons, (2) MM charges were estimated by the QEq[90] method at the lowest energy conformer among about 100 ones obtained in (1) and mechanically embedded in the subsequent ONIOM calculations, and (3) geometry optimization at the ONIOM level was performed from the lowest energy conformer by using an optimizer in the GRRM program coupled with the Gaussian microiteration code. In the μ-*l*ADDF calculation, to complete 15 of the largest ADDF, 45 ADDs were detected on the smallest hypersphere, and the 30 largest ones were followed among the 45. The 30 ADDs were followed simultaneously, and 15 are omitted without completion of the ADDF when the other 15 overcame barriers along their traces. The 15 largest ADDF were completed also in the *l*ADDF calculation for the model system at B3LYP/6-31G(d) level. The μ-*d*ADDF algorithm was also tested.

Figure 2a and b shows TSs and products for bond rearrangements in Si_6-cage backbone of hexasilaprizmane for both the real and the model system, respectively. Only the lowest energy TS is shown in Figure 2 when there are more than one TS for a bond rearrangement in the Si_6-cage due to different (a) hydrocarbon arrangement or (b) H atom direction. Although there are two other reaction pathways with H atom transfer in the model system, they are not shown in Figure 2b for simplicity. Among three TSs in Figure 2b, model-TS3 was taken from previous *f*ADDF results[91] for explanation, although it was not found by the *l*ADDF treating only 15 ADDs because of its high barrier. In Figure 2a, there

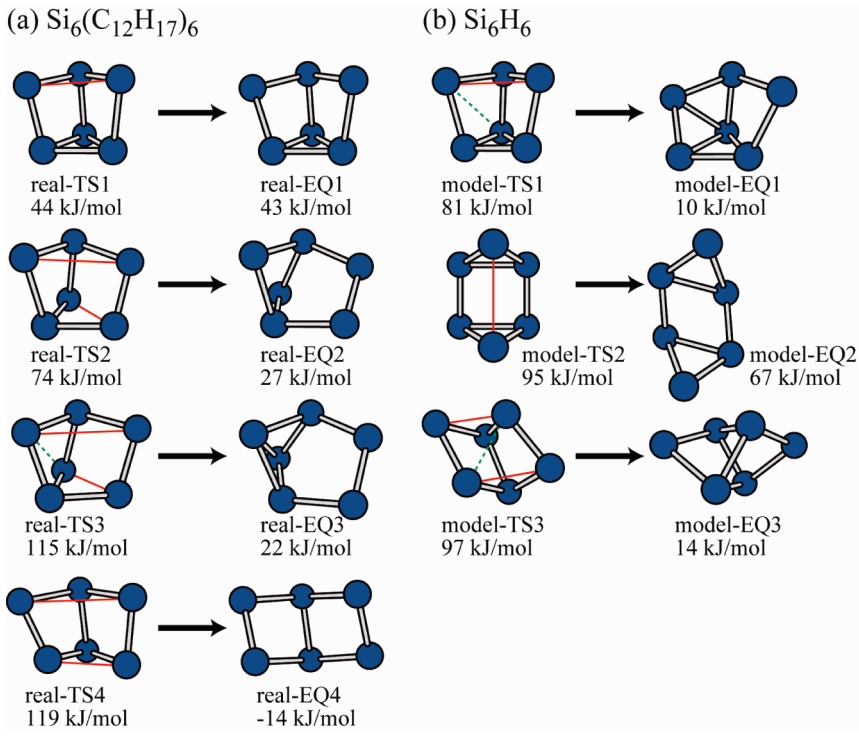

Figure 2. TSs and products of reactions in the Si_6 backbone for (a) $Si_6(C_{12}H_{17})_6$ and (b) Si_6H_6. Every Si atoms have one (a) $C_{12}H_{17}$ or (b) H. Thin (red) lines and dashed (green) lines on TSs show dissociating and generating bonds, respectively.

are four different Si−Si bond-breaking patterns in one of the triangles of the prism, depending on other subsequent bond breaking or formation: (1) the reaction stops after one bond breaking via real-TS1, (2) a backward Si−Si bond in another triangle breaks subsequently via real-TS2, (3) one bond formation accompanies in addition to the two bonds breaking like (2) via real-TS3, which leads to a product with hexasilabenzvalene backbone, (4) a Si−Si bond on the same side of another triangle breaks subsequently via real-TS4, which leads to a product with hexasila-Dewar-benzene backbone. The bond reorganization pattern in model-TS1 is similar to real-TS3, although another bond breaks in real-TS3 to reduce steric repulsion among hydrocarbon substituents in crowded parts. The bond reorganization pattern in model-TS3 is similar to the one in real-TS4, although further bond formation in model-TS3 is prohibited in the real-TS4 because of an increase of steric repulsion due to the bond formation. There are two other TSs in the model system involving H atom transfer from a Si to another Si, and their bond rearrangement pattern in the Si_6 backbone is very similar to both real-TS1 and -TS2, although $C_{12}H_{17}$ transfer in the real system is very difficult because of steric repulsion. A TS similar to model-TS2 was not found in the real system by the *l*ADDF treating of only 15 ADDs. Although it might be found also in the real system if *f*ADDF is performed, we did not do this test because of its high costs. This PES is related to the synthesis of $Si_6(C_{12}H_{17})_6$ with the hexasilaprizmane backbone and the thermal reaction from hexasila-Dewar-benzene to hexasilaprizmane after photolysis of hexasilaprizmane.[86−88] Such experimental studies aimed at synthesis of hexasilabenzene, which have not yet materialized,[92] and PESs between hexasilabenzene and other $Si_6(C_{12}H_{17})_6$ compounds are of great interest in inorganic chemistry. PESs for rearrangements of $Si_6(C_{12}H_{17})_6$ among hexasilaprizmane, hexasila-Dewar-benzene, hexasilabenzvalene, and hexasilabenzene at a higher computation level will be discussed in a forthcoming paper together with their theoretical photoabsorption spectra.

Table 3. Performance of μ-*l*ADDF for $Si_6(C_{12}H_{17})_6$, *l*ADDF for Si_6H_6 (model system), and μ-*d*ADDF for $Si_6(C_{12}H_{17})_6$

	μ-*l*ADDF	*l*ADDF	μ-*d*ADDF-TS (PR[a]-DB[b])	μ-*d*ADDF-TS (PR[a]-BV[c])	μ-*d*ADDF-EQ (DB[b]-BV[c])
n_{ADD}	15	15	1	1	1
$n_{gradient}$	14540	11020	146[d]/147[e]	82[d]/162[f]	189[e]/190[f]
$n_{Hessian}$	937	438	14[d]/16[e]	6[d]/8[f]	8[e]/8[f]

[a] Hexasilaprismane type EQ (see Figure 1). [b] Hexasila-Dewar-benzene type EQ (see real-eq 4 in Figure 2). [c] Hexasilabenzvalene type EQ (see real-eq 3 in Figure 2). [d] PR was the sphere-center. [e] DB was the sphere-center. [f] BV was the sphere-center.

Table 3 shows performance of the μ-*l*ADDF and the *l*ADDF for the real system and the model system, respectively. Since we set the numbers of ADDs to be followed as 15 in the *l*ADDF treatment, n_{ADD} is 15 in both cases. There were many TSs for similar bond rearrangements in Si_6 due to C_1 symmetry in the real system, and this increased the numbers of IRC calculations significantly. Actually, 14 independent TSs were located in the real system, whereas only 5 TSs were located in the model system. In this system, we also tested the μ-*d*ADDF-TS and μ-*d*ADDF-EQ algorithms, which are applied to pathways among hexasilaprizmane, hexasila-Dewar-benzene, and hexasilabenzvalene. Table 3 also shows their performance, where costs for IRC calculations are not included in $n_{gradient}$ and $n_{Hessian}$ for μ-*d*ADDF. In the μ-*d*ADDF, n_{ADD} is always one. Although performance slightly depends on choices of sphere-center

in the μ-*d*ADDF-TS between hexasilaprizmane and hexasila-Dewar-benzene and in the μ-*d*ADDF-EQ between hexasila-Dewar-benzene and hexasilabenzvalene, very different in the μ-*d*ADDF-TS between hexasilaprizmane and hexasilabenzvalene since hexasilabenzvalene is much closer to the TS than hexasilaprizmane. In the μ-*d*ADDF-EQ, hexasilaprizmane was obtained as unique intermediate, and the total cost for obtaining the pathway between hexasila-Dewar-benzene and hexasilabenzvalene by using the μ-*d*ADDF methods is 417−499 gradient and 28−32 Hessian calculations.

$C_6H_{10}O$ in Pure QM Calculations. To see the performance of the μ-*f*ADDF in the pure QM system, we applied it to cyclohexanone (a cyclic ketone molecule with a C_6 ring) at the semiempirical PM3 level, where a carbonyl group and two carbons connected to the carbonyl group ($C_2C{=}O$) were treated as reaction-center atoms. The μ-*f*ADDF traced eight pathways: two isomerization pathways from $C_2C{=}O$ to $C{-}C{-}O{-}C$ with a C_6O seven membered ring via a TS, two C−C bond dissociation pathways to a $(CH_2)_5CO$ diradical chain, a direct oxygen dissociation route, two dissociation routes to cyclopentane + CO via a TS, and a C−C bond dissociation route with a H atom transfer from CH_2 to C═O generating $CH(CH_2)_4CHO$. Here, this result for C_2CO reaction-center is very similar to the H_2CO shown above. The number of macroiterations was 2 081 (1 996 force and 85 Hessian), and this is again comparable to the performance of the *f*ADDF in H_2CO (see Table 2). In full-QM systems, costs of microiterations are not negligible, and 20 096 forces were required in total for microiteration. This implies that microiterations converged with only 10 iterations on average because of the following two reasons: (1) the maximum step size in each macroiteration was limited to 0.1 Å, and (2) the optimizer of Gaussian programs is very efficient. Hence, the numbers of force calculations in the present μ-ADDF applied to full-QM systems can be estimated to be ∼10 times larger than those of the model systems. This is a significant improvement over the *f*ADDF since its cost will increase exponentially depending on the numbers of atoms.

IV. Remarks on Limitations and Future Applications

An upper limit in the numbers of nonreaction-center atoms, which can be handled in the present μ-ADDF algorithm (n_{MAX}), is determined by a memory size for Hessian storage in the transformation of nonreaction-center Hessian to the effective Hessian in eq 10. For example, n_{MAX} will be about 10 000 if available memory size is 8.0 GB. Hence, a small enzyme may be a target of future applications. Further increase of system size can be achieved by an introduction of an approximation in which a part of a huge molecule very far away from a reaction-center is frozen at an initially optimized or experimental geometry. Systematic search for TSs by the μ-ADDF with this approximation will give many candidates of TSs, and then they can be reoptimized in full dimension by using the microiteration-based optimizer in the Gaussian programs. This treatment of dividing a huge molecule into three parts, i.e., reaction-center, nonreaction-center, and frozen atoms, is already available in the GRRM program for future studies, although this approximation was not necessary in the present small systems.

When the numbers of nonreaction-center atoms are less than n_{MAX}, applicability is determined from the numbers of reaction-center QM atoms. Although it will strongly depend on available computer resources and computation levels, we expect from our previous applications that upper limits may be ∼20 atoms for *f*ADDF, ∼50 atoms for *l*ADDF, and >100 atoms in *d*ADDF, for example, with DFT with a double-ζ basis set on eight or more cores of CPU. For example, in general, 100 or more atoms are often treated as a QM system in studies of enzyme reactions to take interactions between reaction-centers and surrounding residues and/or solvents into account. This is too much if a fully automated exploration of potential surface, by using the *l*ADDF, is desired. In this case, use of the three-layer ONIOM(QM/QM/MM) with a semiempirical QM method for a medium layer could be used in an initial search for candidates of TS structures by the *l*ADDF, where such a medium layer will also be treated by the microiteration. Then, they can be refined by using the two-layer ONIOM(QM/MM) and the standard TS optimizer. An application of the present approach to enzyme reactions will be a big challenge in the future.

Recently, we made systematic searches for minima on seams of crossing (MSX) structures possible for nonadiabatic transitions in photochemical and ion−molecule reactions by using the GRRM method.[93] A coupling of the MSX search code with the present μ-ADDF code will be an important development in the future.

V. Conclusion

In this study, we combined the microiteration technique with the GRRM method. Effective Hessian that includes full quadratic couplings between both reaction center and microiteration variables were derived for the reaction center variables. The standard GRRM program was modified so that such an effective Hessian can be employed in the full and large-ADDF GRRM method as well as the double-ended GRRM method on the basis of μ-ADDF algorithm. Their performance was tested for ONIOM calculations for (1) H_2CO surrounded by 100 water molecules and (2) a prism-like Si_6-cage with six ($C_{12}H_{17}$) substituents, where H_2CO and Si_6C_6 were assumed to be reaction center atoms, respectively, as well as the pure QM calculations for cyclohexanone. The number of macroiterations in each application was compared to the number of total steps in similar calculations of the model systems, i.e., isolated H_2CO and Si_6H_6. The number of macroiterations was slightly larger than the number of total steps in the model system due to symmetry lowering (from C_{2v} to C_1) in H_2CO by the surrounding asymmetric $(H_2O)_{100}$ cluster. This effect was larger in the Si_6 case than in H_2CO because of a higher (D_{3h}) symmetry in the model system. Except for this, the μ-ADDF in both $(H_2CO)(H_2O)_{100}$ and $Si_6(C_{12}H_{17})$ worked almost as well as the conventional ADDF in the model systems in spite of flexible environments. Therefore, we conclude that the GRRM method combined with the μ-ADDF algorithm will be a very powerful tool for exploring PESs of reaction-center variables in large molecular systems.

Acknowledgment. S.M. thanks Prof. Takeaki Iwamoto for the helpful discussions about previous experimental studies on hexiasilaprizmane. S.M. is supported by a Research Fellowship of the Japan Society for Promotion of Science for Young Scientists. This work is partly supported by a grant from Japan Science and Technology Agency with a Core Research for Evolutional Science and Technology (CREST) in the Area of High Performance Computing for Multiscale and Multiphysics Phenomena as well as a grant from AFOSR (grant no. FA9550-07-1-0395).

References

(1) Schlegel, H. B. *J. Comput. Chem.* **2003**, *24*, 1514.

(2) Jensen, F. *Introduction to Computational Chemistry*, 2nd ed.; Wiley: Chichester, U.K., 2007.

(3) Warshel, A.; Levitt, M. *J. Mol. Biol.* **1976**, *103*, 227.

(4) Singh, U. C.; Kollman, P. A. *J. Comput. Chem.* **1986**, *7*, 718.

(5) Field, M. J.; Bash, P. A.; Karplus, M. *J. Comput. Chem.* **1990**, *11*, 700.

(6) Svensson, M.; Humbel, S.; Froese, R. D. J.; Matsubara, T.; Sieber, S.; Morokuma, K. *J. Phys. Chem.* **1996**, *100*, 19357.

(7) Dapprich, S.; Komáromi, I.; Byun, K. S.; Morokuma, K.; Frisch, M. J. *THEOCHEM* **1999**, *461−462*, 1.

(8) Morokuma, K. *Bull. Korean Chem. Soc.* **2003**, *24*, 797.

(9) Schlegel, H. B. *J. Comput. Chem.* **1982**, *3*, 214.

(10) Cerjan, C. J.; Miller, W. H. *J. Chem. Phys.* **1981**, *75*, 2800.

(11) Banerjee, A.; Adams, N.; Simons, J.; Shepard, R. *J. Phys. Chem.* **1985**, *89*, 52.

(12) Pulay, P.; Fogarasi, G.; Pang, F.; Boggs, J. E. *J. Am. Chem. Soc.* **1979**, *101*, 2550.

(13) Fogarasi, G.; Zhou, X.; Taylor, P.; Pulay, P. *J. Am. Chem. Soc.* **1992**, *114*, 8191.

(14) Peng, C.; Ayala, P. Y.; Schlegel, H. B.; Frisch, M. J. *J. Comput. Chem.* **1996**, *17*, 49.

(15) (a) Broyden, C. G. *J. Inst. Math. Appl.* **1970**, *6*, 76. (b) Fletcher, R. *Computer Journal (Switzerland)* **1970**, *13*, 317. (c) Goldfarb, D. *Mathematics of Computation* **1970**, *24*, 23. (d) Shanno, D. F. *Mathematics of Computation* **1970**, *24*, 647.

(16) Murtagh, B.; Sargent, R. W. H. *Computer Journal (Switzerland)* **1972**, *13*, 185.

(17) Powell, M. J. D. *Mathematical Programming* **1971**, *1*, 26.

(18) Bofill, J. M. *J. Comput. Chem.* **1994**, *15*, 1.

(19) Golab, J. T.; Yeager, D. L.; Jørgensen, P. *Chem. Phys.* **1983**, *78*, 175.

(20) Helgaker, T. *Chem. Phys. Lett.* **1991**, *182*, 503.

(21) Culot, P.; Dive, G.; Nguyen, V. H.; Ghuysen, J. M. *Theor. Chim. Acta.* **1992**, *82*, 189.

(22) Maseras, F.; Morokuma, K. *J. Comput. Chem.* **1995**, *16*, 1170.

(23) Zhang, Y. K.; Liu, H. Y.; Yang, W. T. *J. Chem. Phys.* **2000**, *112*, 3483.

(24) Murphy, R. B.; Philipp, D. M.; Friesner, R. A. *J. Comput. Chem.* **2000**, *21*, 1442.

(25) Hayashi, S.; Ohmine, I. *J. Phys. Chem.* **2000**, *104*, 10678.

(26) Billeter, S. R.; Turner, A. J.; Thiel, W. *Phys. Chem. Chem. Phys.* **2000**, *2*, 2177.

(27) Hall, R. J.; Hindle, S. A.; Burton, N. A.; Hillier, I. H. *J. Comput. Chem.* **2000**, *21*, 1433.

(28) Vreven, T.; Morokuma, K.; Farkas, Ö.; Schlegel, H. B.; Frisch, M. J. *J. Comput. Chem.* **2003**, *24*, 760.

(29) Vreven, T.; Frisch, M. J.; Kudin, K. N.; Schlegel, H. B.; Morokuma, K. *Mol. Phys.* **2006**, *104*, 701.

(30) Davidson, E. R. *J. Comput. Phys.* **1975**, *17*, 87.

(31) Greengard, L.; Rokhlin, V. *J. Comput. Phys.* **1987**, *73*, 325.

(32) Kudin, K. N.; Scuseria, G. E. *Chem. Phys. Lett.* **1998**, *283*, 61.

(33) Frisch, M. J.; Trucks, G. W.; Schlegel, H. B.; Scuseria, G. E.; Robb, M. A.; Cheeseman, J. R.; Scalmani, G.; Barone, V.; Mennucci, B.; Petersson, G. A.; Nakatsuji, H.; Caricato, M.; Li, X.; Hratchian, H. P.; Izmaylov, A. F.; Bloino, J.; Zheng, G.; Sonnenberg, J. L.; Hada, M.; Ehara, M.; Toyota, K.; Fukuda, R.; Hasegawa, J.; Ishida, M.; Nakajima, T.; Honda, Y.; Kitao, O.; Nakai, H.; Vreven, T.; Montgomery, Jr., J. A.; Peralta, J. E.; Ogliaro, F.; Bearpark, M.; Heyd, J. J.; Brothers, E.; Kudin, K. N.; Staroverov, V. N.; Kobayashi, R.; Normand, J.; Raghavachari, K.; Rendell, A.; Burant, J. C.; Iyengar, S. S.; Tomasi, J.; Cossi, M.; Rega, N.; Millam, J. M.; Klene, M.; Knox, J. E.; Cross, J. B.; Bakken, V.; Adamo, C.; Jaramillo, J.; Gomperts, R.; Stratmann, R. E.; Yazyev, O.; Austin, A. J.; Cammi, R.; Pomelli, C.; Ochterski, J. W.; Martin, R. L.; Morokuma, K.; Zakrzewski, V. G.; Voth, G. A.; Salvador, P.; Dannenberg, J. J.; Dapprich, S.; Daniels, A. D.; Farkas, O.; Foresman, J. B.; Ortiz, J. V.; Cioslowski, J.; Fox, D. J. *Gaussian 09*, Revision A.1; Gaussian, Inc.: Wallingford, CT, 2009.

(34) Lundberg, M.; Kawatsu, T.; Vreven, T.; Frisch, M.; Morokuma, K. *J. Chem. Theory Comput.* **2009**, *5*, 222.

(35) Müller, K.; Brown, L. D. *Theor. Chim. Acta* **1979**, *53*, 75.

(36) Peng, C.; Schlegel, H. B. *Isr. J. Chem.* **1993**, *33*, 449.

(37) Ayala, P. Y.; Schlegel, H. B. *J. Chem. Phys.* **1997**, *107*, 375.

(38) Henkelman, G.; Jónsson, H. *J. Chem. Phys.* **2000**, *113*, 9978.

(39) E, W.; Ren, W.; Vanden-Eijnden, E. *Phys. Rev. B: Condens. Matter* **2002**, *66*, 052301.

(40) Peters, B.; Heyden, A.; Bell, A. T.; Chakraborty, A. *J. Chem. Phys.* **2004**, *120*, 7877.

(41) Quapp, W. *J. Chem. Phys.* **2005**, *122*, 174106.

(42) Maeda, S.; Ohno, K. *Chem. Phys. Lett.* **2005**, *404*, 95.

(43) Maeda, S.; Ohno, K. *J. Chem. Phys.* **2006**, *124*, 174306.

(44) Pancíř, J. *Collect. Czech. Chem. Commun.* **1975**, *40*, 1112.

(45) Basilevsky, M. V.; Shamov, A. G. *Chem. Phys.* **1981**, *60*, 347.

(46) Basilevsky, M. V. *Chem. Phys.* **1982**, *67*, 337.

(47) Rowe, D. J.; Ryman, A. *J. Math. Phys.* **1982**, *23*, 732.

(48) Hoffman, D. K.; Nord, R. S.; Ruedenberg, K. *Theor. Chim. Acta* **1986**, *69*, 265.

(49) Jørgensen, P.; Jensen, H. J. A.; Helgaker, T. *Theor. Chim. Acta* **1988**, *73*, 55.

(50) Quapp, W. *Theor. Chim. Acta* **1989**, *75*, 447.

(51) Schlegel, H. B. *Theor. Chim. Acta* **1992**, *83*, 15.

(52) Sun, J.-Q.; Ruedenberg, K. *J. Chem. Phys.* **1993**, *98*, 9707.

(53) Bondensgård, K.; Jensen, F. *J. Chem. Phys.* **1996**, *104*, 8025.

(54) Quapp, W.; Hirsch, M.; Imig, O.; Heidrich, D. *J. Comput. Chem.* **1998**, *19*, 1087.

(55) Quapp, W.; Hirsch, M.; Heidrich, D. *Theor. Chem. Acc.* **1998**, *100*, 285.

(56) Bofill, J. M.; Anglada, J. M. *Theor. Chem. Acc.* **2001**, *105*, 463.

(57) Crehuet, R.; Bofill, J. M.; Anglada, J. M. *Theor. Chem. Acc.* **2002**, *107*, 130.

(58) Hirsch, M.; Quapp, W. *J. Comput. Chem.* **2002**, *23*, 887.

(59) Dallos, M.; Lischka, H.; Monte, E. V. D.; Hirsch, M.; Quapp, W. *J. Comput. Chem.* **2002**, *23*, 576.

(60) Hirsch, M.; Quapp, W. *J. Mol. Struct. (Theochem)* **2004**, *689*, 1.

(61) Ohno, K.; Maeda, S. *Chem. Phys. Lett.* **2004**, *384*, 277.

(62) Maeda, S.; Ohno, K. *J. Phys. Chem. A* **2005**, *109*, 5742.

(63) Ohno, K.; Maeda, S. *J. Phys. Chem. A* **2006**, *110*, 8933.

(64) Ohno, K.; Maeda, S. *Phys. Scr.* **2008**, *78*, 058122.

(65) Yang, X.; Maeda, S.; Ohno, K. *J. Phys. Chem. A* **2005**, *109*, 7319.

(66) Yang, X.; Maeda, S.; Ohno, K. *Chem. Phys. Lett.* **2006**, *418*, 208.

(67) Yang, X.; Maeda, S.; Ohno, K. *J. Phys. Chem. A* **2007**, *111*, 5099.

(68) Watanabe, Y.; Maeda, S.; Ohno, K. *Chem. Phys. Lett.* **2007**, *447*, 21.

(69) Maeda, S.; Ohno, K. *Chem. Phys. Lett.* **2008**, *460*, 55.

(70) Fukui, K. *Acc. Chem. Res.* **1981**, *14*, 363.

(71) Ishida, K.; Morokuma, K.; Komornicki, A. *J. Chem. Phys.* **1977**, *66*, 2153.

(72) Page, M.; McIver, J. W., Jr. *J. Chem. Phys.* **1988**, *88*, 922.

(73) Gonzalez, C.; Schlegel, H. B. *J. Chem. Phys.* **1989**, *90*, 2154.

(74) Maeda, S.; Ohno, K. *J. Phys. Chem. A* **2007**, *111*, 4527.

(75) Bell, R. P. *Proc. R. Soc. London, Ser. A* **1936**, *154*, 414.

(76) Evans, M. G.; Polanyi, M. *Trans. Faraday Soc.* **1936**, *32*, 1333.

(77) Luo, Y.; Maeda, S.; Ohno, K. *J. Phys. Chem. A* **2007**, *111*, 10732.

(78) Maeda, S.; Ohno, K. *J. Phys. Chem. A* **2008**, *112*, 2962.

(79) Luo, Y.; Maeda, S.; Ohno, K. *J. Comput. Chem.* **2009**, *30*, 952.

(80) Maeda, S.; Ohno, K. *J. Phys. Chem. A* **2007**, *111*, 13168.

(81) Maeda, S.; Ohno, K. *J. Am. Chem. Soc.* **2008**, *130*, 17228.

(82) Maeda, S.; Ohno, K. *Chem. Phys. Lett.* **2003**, *381*, 177.

(83) Miller, W. H.; Handy, N. C.; Adams, J. E. *J. Chem. Phys.* **1980**, *72*, 99.

(84) Frisch, M. J.; Trucks, G. W.; Schlegel, H. B.; Scuseria, G. E.; Robb, M. A.; Cheeseman, J. R.; Montgomery, Jr., J. A.; Vreven, T.; Kudin, K. N.; Burant, J. C.; Millam, J. M.; Iyengar, S. S.; Tomasi, J.; Barone, V.; Mennucci, B.; Cossi, M.; Scalmani, G.; Rega, N.; Petersson, G. A.; Nakatsuji, H.; Hada, M.; Ehara, M.; Toyota, K.; Fukuda, R.; Hasegawa, J.; Ishida, M.; Nakajima, T.; Honda, Y.; Kitao, O.; Nakai, H.; Klene, M.; Li, X.; Knox, J. E.; Hratchian, H. P.; Cross, J. B.; Adamo, C.; Jaramillo, J.; Gomperts, R.; Stratmann, R. E.; Yazyev, O.; Austin, A. J.; Cammi, R.; Pomelli, C.; Ochterski, J. W.; Ayala, P. Y.; Morokuma, K.; Voth, G. A.; Salvador, P.; Dannenberg, J. J.; Zakrzewski, V. G.; Dapprich, S.; Daniels, A. D.; Strain, M. C.; Farkas, O.; Malick, D. K.; Rabuck, A. D.; Raghavachari, K.; Foresman, J. B.; Ortiz, J. V.; Cui, Q.; Baboul, A. G.; Clifford, S.; Cioslowski, J.; Stefanov, B. B.; Liu, G.; Liashenko, A.; Piskorz, P.; Komaromi, I.; Martin, R. L.; Fox, D. J.; Keith, T.; Al-Laham, M. A.; Peng, C. Y.; Nanayakkara, A.; Challacombe, M.; Gill, P. M. W.; Johnson, B.; Chen, W.; Wong, M. W.; Gonzalez, C.; Pople, J. A. *Gaussian 03*, Revision C.02; Gaussian, Inc.: Wallingford, CT, 2004.

(85) Farkas, Ö.; Schlegel, H. B. *J. Chem. Phys.* **1999**, *111*, 10806.

(86) Sekiguchi, A.; Yatabe, T.; Kabuto, C.; Sakurai, H. *J. Am. Chem. Soc.* **1994**, *115*, 5853.

(87) Sekiguchi, A.; Yatabe, T.; Doi, S.; Sakurai, H. *Phosphorus, Sulfur Silicon Relat. Elem.* **1994**, *93*−*94*, 193.

(88) Sekiguchi, A.; Sakurai, H. *Adv. Organomet. Chem.* **1995**, *37*, 1.

(89) Jorgensen, W. L.; Chandrasekhar, J.; Madura, J. D.; Impey, R. W.; Klein, M. L. *J. Chem. Phys.* **1983**, *79*, 926.

(90) Rappé, A. K.; Goddard III, W. A. *J. Phys. Chem.* **1991**, *95*, 3358.

(91) Moteki, M.; Maeda, S.; Ohno, K. *Organometallics* **2009**, *28*, 2218.

(92) Lee, V. Y.; Sekiguchi, A. *Chem. Soc. Rev.* **2008**, *37*, 1652.

(93) Maeda, S.; Ohno, K.; Morokuma, K. *J. Phys. Chem. A* **2009**, *113*, 1704.

CT9003383